



**HAL**  
open science

## **Ln-MOF Based Ratiometric Luminescent Sensor for the Detection of Potential COVID-19 Drugs**

Xinrui Wang, Kamal Batra, Gilles Clavier, Guillaume Maurin, Bin Ding, Antoine Tissot, Christian Serre

► **To cite this version:**

Xinrui Wang, Kamal Batra, Gilles Clavier, Guillaume Maurin, Bin Ding, et al.. Ln-MOF Based Ratiometric Luminescent Sensor for the Detection of Potential COVID-19 Drugs. *Chemistry - A European Journal*, 2023, 29 (12), pp.13978-14007. 10.1002/chem.202203136 . hal-04282793

**HAL Id: hal-04282793**

**<https://hal.science/hal-04282793>**

Submitted on 13 Nov 2023

**HAL** is a multi-disciplinary open access archive for the deposit and dissemination of scientific research documents, whether they are published or not. The documents may come from teaching and research institutions in France or abroad, or from public or private research centers.

L'archive ouverte pluridisciplinaire **HAL**, est destinée au dépôt et à la diffusion de documents scientifiques de niveau recherche, publiés ou non, émanant des établissements d'enseignement et de recherche français ou étrangers, des laboratoires publics ou privés.

# Ln-MOF Based Ratiometric Luminescent Sensor for the Detection of Potential COVID-19 Drugs

Xinrui Wang<sup>[a]</sup>, Kamal Batra<sup>[c]</sup>, Gilles Clavier<sup>[d]</sup>, Guillaume Maurin<sup>[c]</sup>, Bin Ding<sup>\*,[b]</sup>, Antoine Tissot<sup>\*,[a]</sup> and Christian Serre<sup>\*,[a]</sup>

**Abstract:** Countless people have been affected by the COVID-19 pandemic on a global scale. Favipiravir, has shown potential as an effective drug for SARS-CoV-2, attracting scientists' attention. However, overuse of Favipiravir easily leads to serious side effects, requiring real-time monitoring in body fluids. Given this, a new lanthanide metal organic framework (MOF) was prepared under solvothermal conditions from either Eu (Eu-MOF or (1)) or Tb (Tb-MOF or (2)) using the highly delocalized imidazoledicarboxylic acid linker H<sub>2</sub>L (H<sub>2</sub>L = 5-(4-(imidazol-1-yl) phenyl) isophthalic acid) and could be successfully applied to selective optical detection of Favipiravir. In this MOF framework, the organic linker H<sub>2</sub>L provides a high excitation energy transfer efficiency that can sensitize luminescence in lanthanides. In addition, through deliberate tuning of Eu/Tb molar ratio and reaction concentration in the lanthanide framework, ratiometric recyclable luminescent **Eu<sub>x</sub>Tb<sub>1-x</sub>-MOF** nanoparticles with open metal sites have been constructed, which present a high detection sensitivity ( $K_{sv} = 1 \times 10^7 \text{ [M}^{-1}]$ , detection limit is 4.63 nM) for Favipiravir. The detection mechanism is discussed with the help of Density Functional Theory (DFT) calculations that sheds light over the selective sensing of Favipiravir over other related COVID-19 drug candidates. Finally, to explore the practical application of Favipiravir sensing, MOF based thin films have been used for visual detection of Favipiravir and recycled 5 times.

RNA polymerase. This blocks the replication and transcription of viral RNA strands which mainly happen in the human blood. However, overuse of Favipiravir can easily lead to serious side effects such as skin rash, diarrhea, and metabolic interruption. Therefore, it is crucial to design effective methods to detect and control the amount of Favipiravir in patients' bodies to avoid side effects<sup>[3]</sup>.

The detection of COVID-19 drugs is currently carried out by separative techniques such as quantitative thin layer chromatography, gas chromatography, or high-performance liquid chromatography. These techniques exhibit good separation and specificity and enable the simultaneous quantification of several drugs<sup>[1, 4]</sup>. However, these methods suffer from important limitations such as a high cost and complex operating conditions. Further, the drug concentration may be vastly different at the time of collection versus the time of measurement. Several challenges remain open for the construction of an easy-to-handle detection platform for COVID-19 drug molecules in real media with high selectivity, low detection thresholds, and anti-interference capabilities with other molecules. Luminescent sensing can facilitate fast response, easy operation, high sensitivity, and avoid external influence all with a low detection cost. Therefore, it could offer a convenient and reusable device for the visual detection of Favipiravir useful for medical staffs.

[a] Xinrui Wang, Dr. Antoine Tissot, Dr. Christian Serre  
Institut des Matériaux Poreux de Paris  
Ecole Normale Supérieure, ESPCI Paris, CNRS, PSL University,  
75005 Paris, France  
E-mail: [antoine.tissot@ens.psl.eu](mailto:antoine.tissot@ens.psl.eu) / [christian.serre@ens.psl.eu](mailto:christian.serre@ens.psl.eu)

[b] Prof. Bin Ding  
Tianjin Key Laboratory of Structure and Performance for Functional Molecule,  
College of Chemistry  
Tianjin Normal University  
393 Binshui West Road, Tianjin 300387, PR China  
E-mail: [hxydb@mail.tjnu.edu.cn](mailto:hxydb@mail.tjnu.edu.cn)

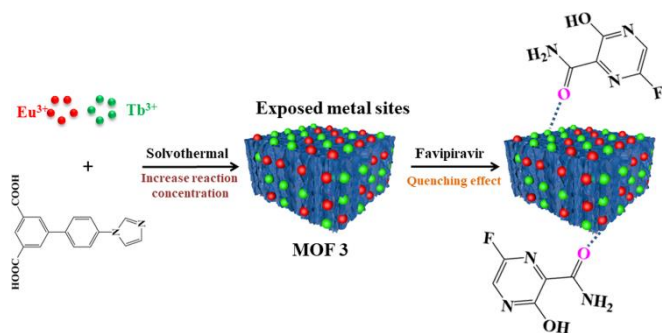
[c] Dr. Kamal Batra, Prof. Guillaume Maurin  
ICGM, Univ. Montpellier, CNRS, ENSCM, Montpellier 34095, France

[d] Dr. Gilles Clavier  
Université Paris-Saclay, ENS Paris-Saclay, CNRS, PPSM, 91190 Gif-sur-Yvette, France.

## Introduction

In recent years, the coronavirus disease 2019 (COVID-19) has rapidly swept the world due to its low fatality rate and its highly infectious character. Countless families have become fragmented because of it, as well as experienced great harm and disruption to our daily lives<sup>[1]</sup>. Favipiravir is a potential effective drug for the treatment of SARS-CoV-2<sup>[2]</sup>. Its mode of action occurs through insertion into the viral RNA chain or binding to the domain of viral

Metal-organic frameworks (MOFs) or porous crystalline hybrid solids, are formed by the coordination between organic ligands and metal cations, oxo-clusters or chains<sup>[5]</sup>. They exhibit features such as high porosity, variable structural motifs<sup>[6]</sup>, adjustable pore size<sup>[7]</sup>, and are of interest for a broad range of potential applications such as gas sorption and separation<sup>[8]</sup>, catalysis<sup>[9]</sup>, biomedicine and sensing<sup>[10]</sup> among others. Lanthanide metal-organic frameworks (Ln-MOFs), a sub-class of MOFs with a great structural diversity associated in some cases with highly porous frameworks, are promising luminescent sensing materials for chemo-sensing that offer several advantages: (i) lanthanides possess strong and narrow characteristic emission peaks<sup>[11]</sup>, as well as long luminescence lifetime and high quantum yield<sup>[12]</sup>. Ln-MOFs emission is enhanced by the antenna effect, corresponding to an excitation energy transfer from the MOF ligand to lanthanide ion<sup>[13]</sup>; (ii) lanthanides have partially filled 4f shells well-shielded from their environment by the closed 5s<sup>2</sup> and 5p<sup>6</sup> shells, which can lead to sensors having a strong resistance to external perturbations<sup>[14-15]</sup>; (iii) in comparison with single lanthanide MOFs, mixed Ln-MOFs can afford ratiometric luminescent sensing platforms<sup>[16-18]</sup>, which can ultimately improve the detection sensitivity and selectivity.



**Scheme 1.** Strategy for Favipiravir luminescent detection by MOF 3.

Compared with single channel based luminescent sensors, ratiometric dual channel luminescent sensors allow for self-correction, which can limit external interferences such as optical occlusion, excitation power fluctuation, atmospheric and pressure effects, thereby improving sensing precision and selectivity<sup>[19-20]</sup>. For example, Cui et al. designed ratiometric luminescence platform based on a boric-acid-functional Eu-MOF for sensitive detection of H<sub>2</sub>O<sub>2</sub> and glucose<sup>[21]</sup>. The proposed method was demonstrated to be highly sensitive and selective for H<sub>2</sub>O<sub>2</sub> and glucose, with the low detection limits of 0.0335 and 0.0643 μM, respectively. Another example was reported by Xu et al. that have designed methyl red@lanthanide metal-organic frameworks (MR@EuMOFs) to monitor food spoilage<sup>[22]</sup>. Here, mixed lanthanide nanocrystals show strong potential in the detection of the targeted analytes. In addition, the use of nanosized MOFs helped to form stable suspensions, which therefore exhibit stable luminescence signals.

In this work, a new Ln-MOF, constructed from either Eu or Tb and an imidazolecarboxylic luminescent ligand, is reported. Its mixed Eu/Tb framework leads to the real-time ratiometric luminescent detection of the COVID-19 drug Favipiravir. The possible coordination mode of Favipiravir towards the lanthanide ions present in the MOF and the resulting electron charge transfer was explored by Density Functional Theory (DFT) calculations. The Favipiravir's sensing mechanism was further evidenced from time resolved luminescence experiments. Finally, as a proof of concept, we have designed a MOF-polymer thin film for optical sensing of Favipiravir, that can be used at least 5 times, which evidences that this material is a practical, recyclable and selective ratiometric luminescent sensing platform.

## Results and Discussion

A three-dimensional (3D) lanthanide nanoMOF has been prepared under solvothermal conditions from the mixture of Ln salts (M = Eu or Tb) and the imidazolecarboxylic acid (H<sub>2</sub>L = 5-(4-(imidazol-1-yl)phenyl)isophthalic acid). The crystal structures have been resolved by single crystal X-Ray diffraction and are constructed either with europium, leading to (1) Eu-MOF [Eu<sub>2</sub>(L)<sub>3</sub>(H<sub>2</sub>O)(DMF)]<sub>n</sub> or with terbium, leading to (2) Tb-MOF [Tb<sub>2</sub>(L)<sub>3</sub>(H<sub>2</sub>O)(DMF)]<sub>n</sub>·H<sub>2</sub>O.

(2). The connection between the Ln centers and the carboxylate and nitrogen groups lead to a 3D framework exhibiting very narrow pores. Additionally, the Eu/Tb ratio has been tuned, leading to a series of mixed-lanthanide frameworks **Eu<sub>0.047</sub>Tb<sub>0.953</sub>-MOF (3)**, **Eu<sub>0.924</sub>Tb<sub>0.076</sub>-MOF (4)** and **Eu<sub>0.526</sub>Tb<sub>0.474</sub>-MOF (5)**. The nanoparticle size of **3** was adjusted by changing the reaction concentration.

Single crystal X-ray diffraction analysis shows that both **1-2** are isostructural and crystallize in a triclinic system with P-1 space group (Table S1). For the sake of clarity, only the structure of **1** is described here (Figure 1; see Figure S1 for structure of **2**). The asymmetric unit of **1** (Figure 1a) contains two Eu<sup>3+</sup> centers (Eu1 and Eu2), three fully deprotonated linker L<sup>2-</sup>, one terminal coordinated water molecule and one terminal coordinated DMF. Each central Eu1 is nine-coordinated by seven oxygen atoms (O1, O2, O2A, O3, O4, O5, O6) from L<sup>2-</sup>, one terminal coordinated H<sub>2</sub>O (O14) and one nitrogen atom (N2) from L<sup>2-</sup> (Figure 1b), while Eu2 is also nine-coordinated by seven oxygen atoms (O7, O8, O9, O9B, O10, O11, O12) from L<sup>2-</sup>, one terminal coordinated DMF (O13) and one nitrogen atom (N4) from L<sup>2-</sup>. Selected bond lengths and angles of **1-2** are summarized in Table S2-S5. The Eu-O bond lengths range from 2.344 Å to 2.743 Å and O-Eu-O bond angles range from 50.01° to 149°, which fall into the usual range for lanthanide compounds<sup>[19]</sup>. Additionally, two Eu atoms (Eu1 and Eu1A or Eu2 and Eu2A) are interlinked via oxygen atoms from the carboxylate group forming dinuclear Eu<sub>2</sub>O<sub>2</sub> oxo-clusters that can be considered as secondary building units (SBUs). On the other hand, each fully deprotonated L<sup>2-</sup> linker has three neighboring dinuclear Eu<sup>3+</sup> SBUs with multidentate bridging mode (Figure 1b), which ultimately constructs the 3D oxocluster-based microporous coordination framework **1** (Figure 1c). Ln...Ln shortest contacts are 4.1 Å from the crystal structures, meaning that adjacent excited Ln centers can electronically communicate<sup>[20]</sup>.

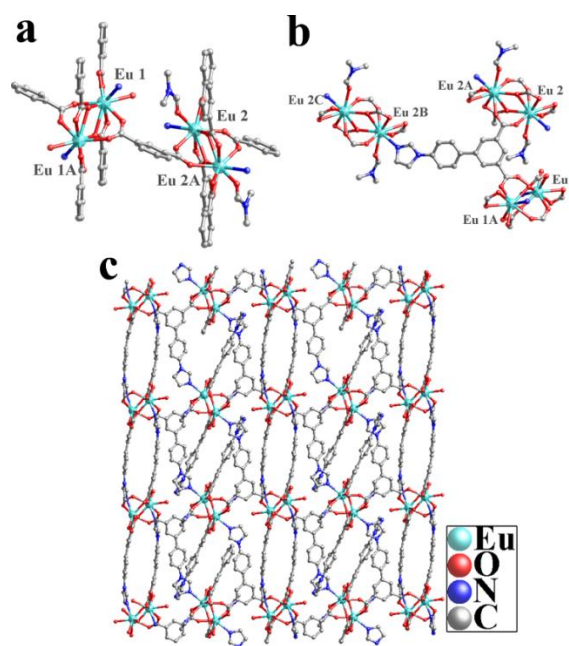


**Figure 1.** (a) fundamental coordination unit of **Eu-MOF (1)**; (b) each L<sup>2-</sup> are linked by three neighboring Eu<sub>2</sub>O<sub>2</sub> SBUs; (c) three-dimensional cluster-based micro-porous structure of **Eu-MOF (1)**.

This is important in a Ln-MOF setting as it can promote energy cascading from Tb<sup>3+</sup> to Eu<sup>3+</sup>, resulting in brightening of Eu<sup>3+</sup> and Tb<sup>3+</sup> luminescence and further improve the sensitivity of the detection system. The coordinated water molecules, carbon atoms and oxygen atoms of ligand L<sup>2-</sup> are involved in intermolecular C-H...O hydrogen bonds (Table S6-S7). Such weak interactions play a crucial role in stabilizing the whole network. The Ln...Ln distances (Ln corresponds to lanthanide) observed along the crystallographic c axis are 15.3 Å × 4.1 Å for **1** and 14.6 Å × 4.1 Å for **2**. According to the Platon program, **1** and **2** present limited solvent accessible void fractions of 7.3 % and 6.9 %, respectively. This shows that these MOFs are almost non-porous further confirmed by absorption of p-diiodobenzene investigated by UV-vis spectrum (Figure S2), suggesting that guest molecules can hardly go inside the pores of these MOFs. UV-vis absorption tests were carried out with Favipiravir, confirming that this molecule cannot get inside the micropores of **3** (Figure S3).

The purity of the as-synthesized samples was verified by powder X-ray diffraction (PXRD) (Figure S4). PXRD patterns of MOFs **1-5** are identical to the simulated patterns from the single-crystal structure and **3** remain stable in the human serum solution with Favipiravir. Inductively coupled plasma (ICP) analysis was used to evaluate the ratio of Eu<sup>3+</sup> and Tb<sup>3+</sup> in MOF **3-5** (Table S8). Transition electron microscopy (TEM) coupled with EDS mapping were performed and show that Eu<sup>3+</sup> and Tb<sup>3+</sup> are uniformly dispersed in larger MOF crystals (Figure 2 and S13-S14). MOFs **1-3** were also characterized by UV-vis absorption spectroscopy, Fourier transform infrared spectroscopy (FT-IR), thermogravimetric analysis (TGA) analysis, variable temperature X-ray diffraction (XRD) and zeta potential measurements (Figure S5-S6). MOFs **1-5** exhibit strong and narrow photo-luminescent emissions, fulfilling the criteria for excellent sensing devices (Scheme 1). **Eu-MOF (1)** has two main and strong emission peaks located at 591 and 618 nm (Figure S7) attributed to <sup>5</sup>D<sub>0</sub>→<sup>7</sup>F<sub>1</sub> and <sup>5</sup>D<sub>0</sub>→<sup>7</sup>F<sub>2</sub> transitions<sup>[21]</sup>. **Tb-MOF (2)** has four emission peaks located at 489, 543, 583 and 618 nm (Figure S8), attributed to <sup>5</sup>D<sub>4</sub>→<sup>7</sup>F<sub>J</sub> (J=3-6) transitions<sup>[21]</sup>. **3** exhibits the emission of both Eu and Tb ions and can therefore be considered as a ratiometric luminescent sensing material, presenting strong emissions at 543 and 617 nm, with CIE coordinates located in the orange region (Figure S9), similarly to previous works<sup>[23]</sup>. To confirm that MOF **3** can be used as luminescent sensor, we have compared it with Eu/Tb-BDC (BDC= 1,3-benzenedicarboxylate) as this dense MOF possesses a similar SBU<sup>[19]</sup> (Figure S10). Eu/Tb-BDC suspensions presented much weaker emission peaks originating from Eu<sup>3+</sup> and Tb<sup>3+</sup> (Figure S11) compared to **3**. This lower emission intensity is likely attributed to a weaker energy transfer from the ligand to metal in Eu/Tb-BDC, while **3** shows very strong luminescent emission. Additionally, the relative quantum yield for Eu/Tb-BDC is 0.02%, as compared to MOF **3** which was used as a reference. The absolute luminescence quantum yields are 11.5% for Eu-MOF (**1**), 15.3% for Tb-MOF (**2**) and 14.6% for **3**. The high quantum yield of MOF **1-3** can be ascribed to the strongly conjugated backbone of H<sub>2</sub>L that is constructed with imidazole and bi-phenyl aromatic moieties and short Ln...Ln distances that may lead to energy transfer between Ln ions, paving the way to an improved sensitivity of the detection system<sup>[24-25]</sup>. Lifetime measurements were taken at 617 and 543 nm corresponding to Eu<sup>3+</sup> and Tb<sup>3+</sup> emission respectively in single metal and all bimetallic Ln-MOFs (MOF **3-5**) (Figure S12). In the latter, the <sup>5</sup>D<sub>4</sub> (Tb<sup>3+</sup>) lifetime is shorter than in pure Tb-MOF (**1**) (250 μs) and the <sup>5</sup>D<sub>0</sub> (Eu<sup>3+</sup>) lifetime is longer than in pure Eu-MOF **2** (460 μs),

suggesting the presence of Tb<sup>3+</sup>-to-Eu<sup>3+</sup> excitation energy transfer process (Figure S12).

To obtain a suspension of MOF **3** with a stable luminescent signal in liquid phase, the MOF particle size was tuned, which can also influence the interaction with the drugs at the surface of MOFs nanoparticles. Compared to the pristine Eu<sub>x</sub>Tb<sub>1-x</sub>MOF, reducing the particle size is hypothesized to increase the proportion of accessible sites at the nanoparticles surface by increasing the concentration of reactor, which may enhance the sensing sensitivity. By tuning the experimental conditions, we obtained nanoparticles of **3** with an average size of 135 nm as observed by SEM and TEM images (Figure 2). We first evaluated the potential of **3** as a ratiometric sensor for several potential COVID-19 drugs. After adding 30 μM of different drugs (Favipiravir, Oseltamivir, Ritonavir, Lopinavir, and chloroquine) into a suspension of **3** (0.1g/L, 1 mL), only Favipiravir induced a strong quenching effect (Figure 3). After immersion into a Favipiravir solution where human serum used as solvent, **3** remains remarkably stable 1 day as indicated by PXRD (Figure S4).

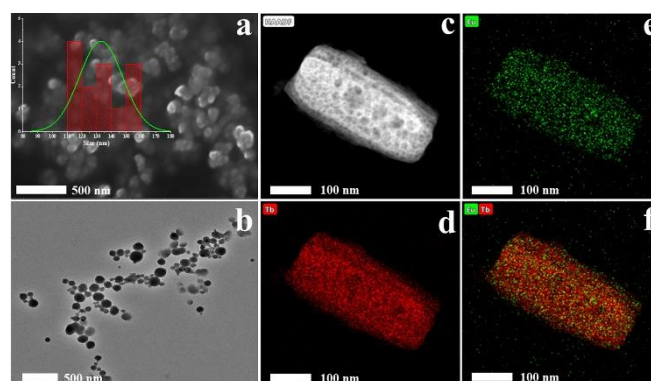


**Figure 2.** (a) SEM image of (a) MOF **3** (insert: nanoparticle size distribution of MOF **3**, average size: 135 nm); (b) TEM image of MOF **3**; (c)-(f) TEM mapping images of MOF **3** crystals.

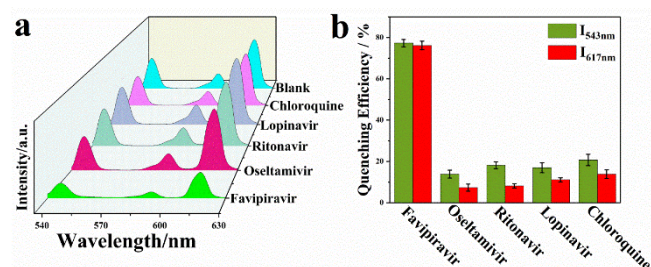
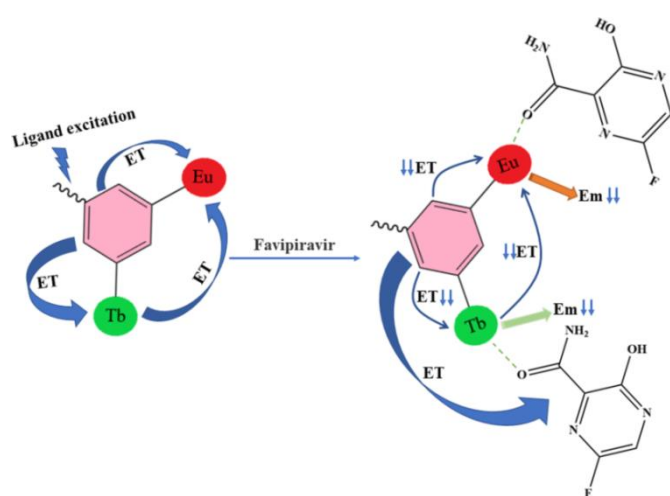


**Figure 3.** (a) Luminescence spectra of **3** before (blank) and after adding Favipiravir, Oseltamivir, Ritonavir, Lopinavir, and Chloroquine respectively (excitation position: 330 nm) in the DMSO solution, test interval: 5 min; (b) quenching efficiency of covid-19 drugs (Favipiravir, Oseltamivir, Ritonavir, Lopinavir, Chloroquine) towards **3**.

The detection sensitivity of **3** was investigated with different concentrations of Favipiravir. A linear relationship between concentration of Favipiravir and luminescence intensity ratio of **3** was obtained:  $I_{617nm}/I_{543nm}=0.01C+1.31$  ( $R^2 = 0.992$ ) (Figure S13), where C corresponds to the concentration of analyte (test

concentration range is 0-28 nM) and  $I_{617\text{nm}}/I_{543\text{nm}}$  is the luminescence intensity ratio between the bands located at 617 and 543 nm. The quenching constant  $K_{\text{sv}}$  was evaluated at  $1 \times 10^7$  [ $\text{M}^{-1}$ ]. It is worth noting the limit of detection (LOD) for Favipiravir is 4.63 nM (Table S9) according to the relation:  $\text{LOD} = 3S_0/S$  (where  $S_0$  is the standard deviation for the blank and  $S$  is the slope of the calibration curve) and the LOD for Favipiravir in this work is far lower than in other reported works (Table S9). Quantitative results in solution exhibited a recovery range from 95.2% to 105.1% with relative standard deviations (RSD) below 1.2% (Table S10). Pure Eu-MOF (1) and Tb-MOF (2) were also tested to detect Favipiravir (Figure S14-S15). Although both show good sensitivity, the associated  $K_{\text{sv}}$  values are  $9 \times 10^6 \text{ M}^{-1}$  for MOF 1 and  $9.3 \times 10^6 \text{ M}^{-1}$  for MOF 2, 3 is a superior sensing platform because it is a self-correcting ratiometric sensor, improving the stability and reliability of detection system.



**Scheme 2.** Main sensing mechanism in Favipiravir detection. ET = energy transfer, Em = Emission.

The detection mechanism of 3 towards Favipiravir has been considered following several aspects. First, pure human serum was added into a suspension of 3, and only induced weak quenching (Figure S16), so the main origin of the large luminescence decrease of MOF 3 should be attributed to Favipiravir. Secondly, the structure of Favipiravir includes a pyrazine with fluorine and amide substituents. It is thus a good acceptor that could be involved in resonance energy transfer (FRET) that may happen at the MOF surface thanks to interactions between Favipiravir and ligand  $L^2$  (Scheme 2 and Figure S17). In such case, the energy donor is ligand  $L^2$  and the energy acceptor Favipiravir as evidenced by the overlap between adsorption spectrum of Favipiravir and luminescent emission spectrum of MOF 3 (Figure S5a and Figure S9c). We have compared the luminescence spectra of Favipiravir and MOF 3 alone and the mixtures of MOF 3 and Favipiravir at the same concentration (Figure S25). The emission of Favipiravir is increased while the emission of the ligand in MOF 3 is decreased when they are mixed compared to their emission intensities alone, which is a clear indication of FRET occurring between them. We have shown that after gradually adding the drug, the lifetime of MOF 3 measured at 370 nm decreased from 1.1 ns to 0.93 ns, while the lifetime of Favipiravir at 430 nm after the addition of increasing amounts of MOF 3 suspension increased from 5.32 ns to 5.46 ns (Table S11-S12, Figure S18). These experimental results confirm that FRET

occurs during the detection progress (scheme 2). Third, according to the luminescence decay recorded after adding Favipiravir into suspensions of Eu-MOF, Tb-MOF and MOF 3 respectively (excitation at 266 nm, Table S13-S16), it appears that the quenching effect of Favipiravir on  $\text{Eu}^{3+}$  and  $\text{Tb}^{3+}$  emission is different in MOF 3 compared to Eu-MOF and Tb-MOF. In details, the luminescence lifetime of  $\text{Tb}^{3+}$  at 543 nm decreased from 186.6  $\mu\text{s}$  to 106.9  $\mu\text{s}$ , while it decreased from 117.3  $\mu\text{s}$  to 100.3  $\mu\text{s}$  in MOF 3. Similarly, the luminescence lifetime of  $\text{Eu}^{3+}$  at 617 nm decreased from 89.7  $\mu\text{s}$  to 80.4  $\mu\text{s}$  in Eu-MOF while it decreased from 199.3  $\mu\text{s}$  to 116.1  $\mu\text{s}$  in MOF 3 (Figure S19). This can be ascribed to the fact that Favipiravir interrupts the energy transfer from the ligand to the metal centers as well as the  $\text{Tb}^{3+}$  to  $\text{Eu}^{3+}$  energy transfer (Scheme 2).

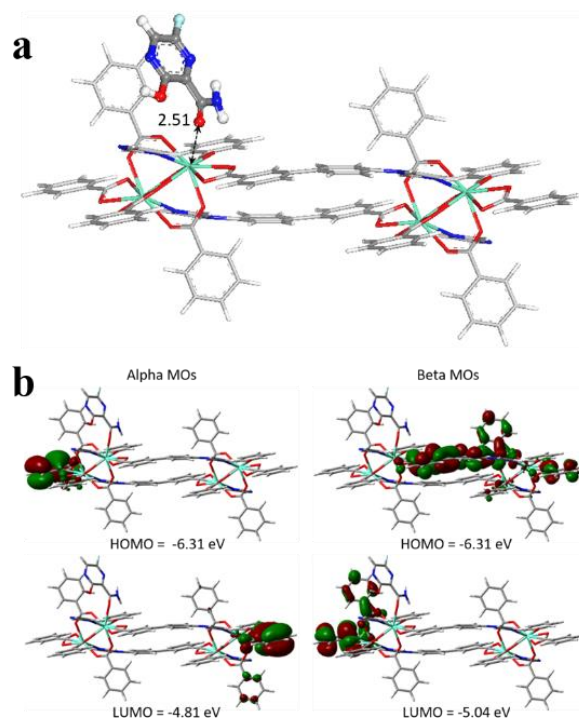


**Figure 4.** (a) DFT optimized geometry of the Favipiravir molecules (ball and stick) interacting with the Eu-MOF cluster (stick). The characteristic interacting distances are reported in Å. Color code for all atoms: hydrogen (white), carbon (light grey), nitrogen (blue), oxygen (red), fluorine (cyan), europium (turquoise); (b) The alpha and beta frontier molecular orbital (the highest occupied molecular orbital and lowest unoccupied molecular orbital, HOMO and LUMO) diagrams for the Favipiravir/MOF cluster (stick). In the MOs, red and green colors indicate the negative and positive charges respectively.

DFT calculations were further performed on Eu-MOF (MOF-1) cluster model that mimics the external surface environment of the metal sites acting as potential adsorption sites for Favipiravir. Figure 4a reveals that the guest molecules adopt a preferential orientation in such a way to interact with Eu sites via its carbonyl group associated with a relatively short  $\text{O}_{(\text{CO}, \text{Fav})}-\text{Eu}$  distance of about 2.5 Å. This observation remains valid starting with an initial geometry implying a dual host-guest interaction via both carbonyl and hydroxyl function of Favipiravir. This is likely associated with high coordination number of Eu as compared to previously reported exposed metal in doped fullerene that prevent chelation geometry [23]. This resulting geometry leads to high calculated interaction energy of -84.2 kJ/mol,

in line with the good Favipiravir/Eu-MOF affinity observed experimentally. Frontier molecular orbitals were further analyzed to characterize the stability of the Favipiravir/Eu MOF complex. Figure 4b reports the charges density localization and energy transport within the alpha and beta MOs of the Favipiravir/Eu MOF complex. For both MOs, HOMOs are associated with similar energy (-6.31 eV) and exhibit a total charge density localized over the imidazole and phenyl rings (Figure 4b). The energies of the LUMOs do not significantly differ (-4.81 eV and -5.04 eV) and the charge density is transferred within the metal-oxo cluster. This later observation suggests that the Favipiravir/Eu-MOF interaction is mainly of physisorption nature since no charge-transfer process is observed.

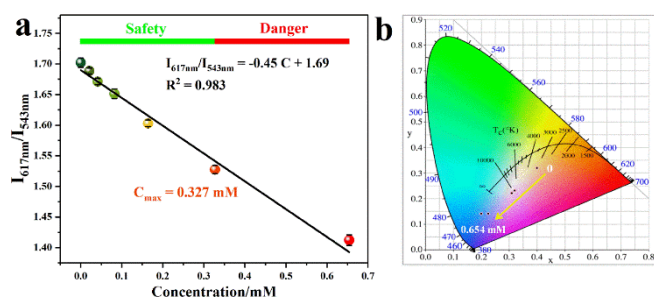


**Figure 5.** (a) Linear relationship between concentration of Favipiravir and luminescence intensity ratio of **3** in human serum solution (5%), test interval: 5 min; (b) CIE coordinates of MOF **3** before and after adding various amounts of Favipiravir.

To explore practical application, we have investigated the sensing potential of **3** in the concentration range when Favipiravir becomes too toxic in human body (indicated by the maximum plasma concentration  $C_{max}$ ). Interestingly, as shown in Figure 5a-b, a linear relationship between luminescence intensity ratio ( $I_{617nm}/I_{543nm}$ ) and Favipiravir concentration was also obtained in the range that contains the  $C_{max}$ . To go further into the real application, a 9.5  $\mu$ m thick polymer composite film **3@PVDF** has been prepared and characterized by laser scanning confocal microscopy (Figure 6 a-c and m) and SEM (Figure S21). It indicates that the luminescence originating from MOF **3** is evenly distributed in the film. PXRD pattern of **3@PVDF** confirmed that the MOF structure is retained (Figure S22). Additionally, after adding different concentrations of Favipiravir, the variation of luminescence intensities is observed by confocal microscopy. Upon contact with Favipiravir, the luminescence in red and green channels decreases, while concomitantly the luminescence in the blue channel due to the Favipiravir increases (Figure 6). This agrees with the sensing mechanism where the ligand transfers its excited state energy to Favipiravir that emits and borrows some energy that is less available for the Ln sensitization that are less emissive. Even though confocal microscopy is less accurate for Favipiravir quantification at low concentration than luminescence spectroscopy, preparing **MOF3@PVDF** films can be convenient for a visual detection of the Favipiravir concentration around  $C_{max}$ . Indeed, differences are easy to observe under UV light adding different amounts of Favipiravir on the film (Figure 7a-e). Noteworthy, this sensor is renewable (Figure 7f), and after added Favipiravir (0.375 mM) can be used at least five times without any decrease of efficiency (Figure S23-S27).

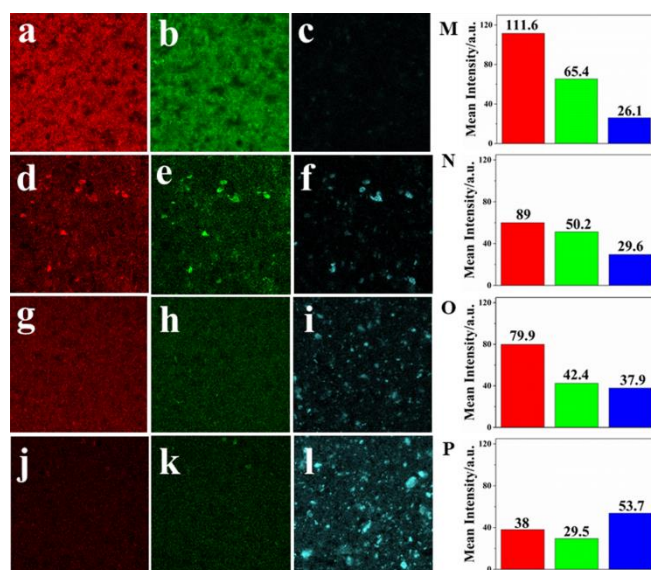


**Figure 6.** Luminescence microscopy images of **MOF3@PVDF**: (a)-(c) before adding Favipiravir in the red, green and blue channels respectively; (d)-(f) after adding 0.021 mM Favipiravir in the red, green and blue channels respectively; (g)-(i) after adding 0.084 mM of Favipiravir in the red, green and blue channels respectively; (j)-(l) after adding 0.375 mM of Favipiravir in the red, green and blue channels respectively; (m) mean intensity of **MOF3@PVDF** in the red, green and blue channels respectively; (n) mean intensity of **MOF3@PVDF** after adding 0.021 mM of Favipiravir in the red, green, and blue channels respectively; (o) **MOF3@PVDF** after adding 0.084 mM of Favipiravir in the red, green, and blue channels respectively; and (p) **MOF3@PVDF** after adding 0.375 mM of Favipiravir in the red, green, and blue channels respectively.

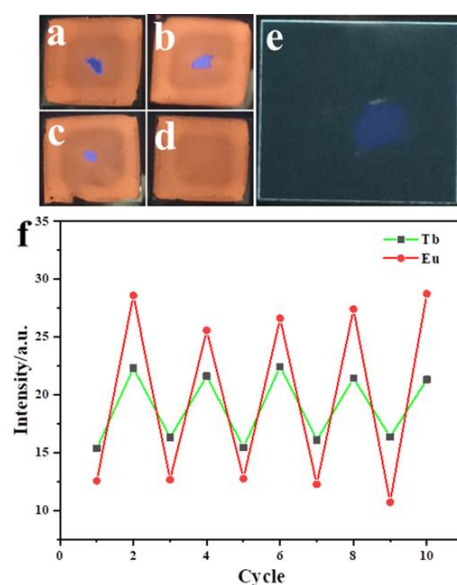


**Figure 7.** Images of **MOF3@PVDF** after adding (a) 0.321 mM; (b) 0.084 mM and (c) 0.041 mM of Favipiravir and (d) without Favipiravir; (e) image of 0.321 mM Favipiravir directly deposited on a glass substrate under UV light (365nm). (f) cycling of **MOF3@PVDF** exposed to Favipiravir (0.375 mM) based on confocal microscopy.

## Conclusion

In conclusion, we report the first ratiometric luminescent sensor based on a new water stable Ln-MOF offering high sensitivity and selective detection towards the potential COVID-19 drug Favipiravir. The associated MOF-drug quenching effect is found to be selective towards other potential COVID-19 drugs. Luminescence decays indicate that FRET is the key parameter for the Favipiravir selective detection. To enable a stable detection system in human serum, the MOF nanoparticle size has been tuned to enhance the sensitivity towards Favipiravir. Finally, as a proof of concept, a MOF-polymer thin film sensing device has been successfully prepared, exhibiting very good detection of Favipiravir as well as excellent reusability (5 times at least). These results pave the way for the development of novel detection devices for COVID-19 drugs via luminescent MOFs, facilitating the discovery of new potential COVID-19 drugs.

## Experimental Section

### Preparation of [Eu<sub>2</sub>(L)<sub>3</sub>(H<sub>2</sub>O)(DMF)]<sub>n</sub> (1).

A mixture of Europium chloride (18.3 mg, 0.05 mmol) and H<sub>2</sub>L (15.4 mg, 0.05 mmol) was added into the mixture of DMF (4 mL) and H<sub>2</sub>O (3 mL). The solution was sealed in a 25 mL Teflon reactor and the reaction mixture was heated at 120 °C for one day and then cooled to room temperature. Colorless bulky crystals of **1** were isolated in 68 % yield based on H<sub>2</sub>L ligand. Elemental analysis found (%) for C<sub>54</sub>H<sub>39</sub>Eu<sub>2</sub>N<sub>7</sub>O<sub>14</sub>: C 49.1 H 2.92 N 7.36; calcd: C 49.36, H 2.99, N 7.46. FT-IR data (cm<sup>-1</sup>): 3642 (w), 3141(w), 1647 (m), 1612(m), 1456 (s), 1421 (s), 1369 (vs), 784(vs), 729 (vs).

### Preparation of [Tb<sub>2</sub>(L)<sub>3</sub>(H<sub>2</sub>O)<sub>2</sub>(DMF)]<sub>n</sub> (2).

A mixture of Terbium chloride (18.7 mg, 0.05 mmol) and H<sub>2</sub>L (15.4 mg, 0.05 mmol) was added into the mixture of DMF (2 mL) and H<sub>2</sub>O (0.5 mL). The solution was sealed in a 25 mL Teflon reactor and the reaction mixture was heated at 120 °C for one day and then cooled to room temperature. Colorless bulky crystals of **2** were isolated in 54 % yield based on H<sub>2</sub>L ligand. Elemental analysis found (%) for C<sub>108</sub>H<sub>82</sub>N<sub>14</sub>O<sub>30</sub>Tb<sub>4</sub>: C 47.98 H 2.96 N 7.18; calcd: C 48.19, H 3.07, N 7.28. FT-IR data (cm<sup>-1</sup>): 3642 (w), 1648 (w), 1618 (m), 1585 (w), 1582 (m), 1446 (s), 1413 (s), 1297 (w), 1052 (w), 774 (s).

### Preparation of Eu<sub>0.047</sub>Tb<sub>0.953</sub>-MOF (3).

A mixture of Europium chloride (2.7 mg, 40.1 nmol), Terbium chloride (53.1 mg, 0.2 mmol) and H<sub>2</sub>L (46.2 mg, 0.15 mmol) was added into the mixture of DMF (1 mL) and H<sub>2</sub>O (0.7 mL). The solution was sealed in a 25 mL Teflon reactor and the reaction mixture was heated at 120 °C for one day and then cooled to room temperature. Colorless bulky crystals of **3** were isolated in 63 % yield based on H<sub>2</sub>L ligand.

### Preparation of Eu<sub>0.924</sub>Tb<sub>0.076</sub>-MOF (4).

A mixture of Europium chloride (17 mg, 0.07 mmol), Terbium chloride (0.9 mg, 3.39 μmol) and H<sub>2</sub>L (15.4 mg, 0.05 mmol) was added into the mixture of DMF (2 mL) and H<sub>2</sub>O (1 mL). The solution was sealed in a 25 mL Teflon reactor and the reaction mixture was heated at 120 °C for one day and then cooled to room temperature. Colorless bulky crystals of **4** were isolated in 66 % yield based on H<sub>2</sub>L ligand.

### Preparation of Eu<sub>0.526</sub>Tb<sub>0.474</sub>-MOF (5).

A mixture of Europium chloride (13 mg, 0.05 mmol), Terbium chloride (13 mg, 0.05 mmol) and H<sub>2</sub>L (15.4 mg, 0.05 mmol) was added into the mixture of DMF (2 mL) and H<sub>2</sub>O (0.7 mL). The solution was sealed in a 25 mL Teflon reactor and the reaction mixture was heated at 120 °C for one day and then cooled to room temperature. Colorless bulky crystals of **5** were isolated in 55 % yield based on H<sub>2</sub>L ligand.

### Preparation of MOF3@PVDF membrane

1.9 g polyvinylidene difluoride (PVDF) was mixed with 20 mL of DMF under stirring for 2h. Then, 10 mg of MOF **3** was added and left under stirring for 12 h. Films were prepared by depositing 0.5 mL of the suspension on a glass substrate with spin coating 800 r/min during 40s.

### Preparation of MOF 3 suspension

To make the suspension of MOF **3**, 1 mg MOF **3** was added 10 mL redistilled water under ultrasonic bath 10 minutes, leading to a stable suspension that has been used for the sensing experiments.

## Supporting Information

Information on synthesis, characterization, structural determination of MOFs and other related information and Crystal data for MOFs.

## Acknowledgements

Xinrui Wang is grateful for the support from CSC grant (grant number: 201908120131). Xinrui Wang appreciates Shi Yangfan and Wang Qian's help for the TEM imaging and thanks for Bernard Goetz for his assistance for ICP tests. Xinrui Wang appreciates the contribution from Jed LaCoste and Ling Fei (University of Louisiana at Lafayette, Madison Hall, Room 218 C, Lafayette, LA, 70504, United States) for the manuscript revision. The computational work was performed using HPC resources from GENCI-CINES (Grant A0100907613).

## Keywords

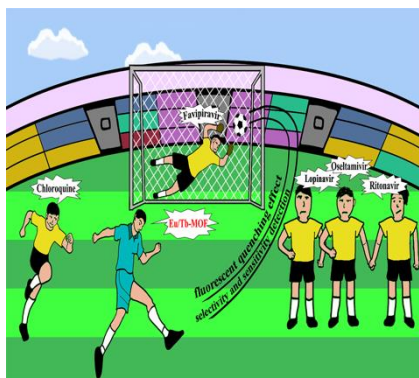
nanoparticles, MOF, ratiometric luminescent sensor, lanthanide, favipiravir, COVID-19

## References

- [1] D. Mathew, J. Giles, Baxter, A. Giles, D. Oldridge, A. Greenplate, J. Wu, C. Alanio, L. Kuri-Cervantes, M. Pampena, K. D'Andrea, S. Manne, Z. Chen, Y. J. Huang, A. Weisman, C. Ittner, O. Kuthuru, J. Dougherty, K. Nzingha, N. Han, J. Kim, A. Pattekar, E. Goodwin, E. Anderson, M. Weirick, S. C. Gouma, M. Bolton, F. Chen, S. Lacey, H. Ramage, S. Cherry, S. Hensley, S. Apostolidis, A. Huang, L. Vella, M. Betts, N. Meyer, E. Wherry, U. C. P. Unit, *Science* **2020**, 369, 1210-1220.
- [2] A. Awadasseid, Y. Wu, Y. Tanaka, W. Zhang, *Biomedicine & Pharmacotherapy* **2021**, 137, 111330-111341.
- [3] P. Eloy, C. Solas, F. Touret, F. Mentre, D. Malvy, X. de Lamballerie, J. Guedj, *Clinical Pharmacology & Therapeutics* **2020**, 108, 188-188.
- [4] Z. Bilgin, I. Evcil, D. Yazgi, G. Binay, C. Genc, B. Gulsen, A. Huseynova, A. Ozdemir, E. Ozmen, Y. S. Usta, S. Andac, *Journal of Chromatographic Science* **2021**, 59, 748-757.
- [5] P. Rouschmeyer, N. Guillou, C. Serre, G. Clavier, C. Clavier, P. Audebert, E. Elkaim, C. Allain, T. Devic, *Inorganic Chemistry* **2017**, 56, 8423-8429.
- [6] T. Devic, C. Serre, N. Audebrand, J. Marrot, G. Férey, *J. Am. Chem. Soc.* **2005**, 127, 12788-12789.
- [7] G. Férey, C. Mellot-Draznieks, C. Serre, F. Millange, J. Dutour, S. Surblé, I. Margiolaki, *Science* **2005**, 309, 2040-2042.
- [8] J. W. Yoon, Y. K. Seo, Y. K. Hwang, J. S. Chang, H. Leclerc, S. Wuttke, P. Bazin, A. Vimont, M. Daturi, E. Bloch, P. L. Llewellyn, C. Serre, P. Horcajada, J. M. Grenèche, A. E. Rodrigues, G. Férey, *Angew. Chem. Int. Ed.* **2010**, 49, 5949-5952.
- [9] P. Horcajada, S. Surblé, C. Serre, D. Y. Hong, Y. K. Seo, J. S. Chang, J. Grenèche, I. Margiolaki, G. Férey, *Chem. Commun.*, **2007**, 27, 2820-2822.
- [10] A. M. L. Marcella, F. L. O. Marina, A. M. Arouca, M. Talhavini, E. A. Ferreira, S. A. Júnior, F. H. Veiga-Souza, I. T. Weber, *ACS Appl. Mater. Interfaces* **2017**, 9, 4684-4691.
- [11] C. Liu, Q. Sun, L. Lin, J. Wang, C. Zhang, C. Xia, T. Bao, J. Wan, R. Huang, J. Zou, *Nature Communications* **2020**, 11, 4971-4979.

- 
- [12] Q. Liu, S. Zhang, J. Yang, K. Yue, *Analyst* **2019**, *144*, 4534-4544
- [13] C. Li, J. Huang, H. Zhu, L. Liu, Y. Feng, G. Hu, X. Yu, *Sensors and Actuators B-Chemical* **2017**, *253*, 275-282..
- [14] B. Yan, *Accounts of Chemical Research* **2017**, *50*, 2789-2798
- [15] C. Serre, F. Millange, C. Thouvenot, F. Gardant, G. Férey, *J. Mater. Chem.* **2004**, *14*, 1540-1543.
- [16] S. Y. Wu, H. Min, W. Shi, P. Cheng, *Adv. Mater.* **2020**, *32*, 1805871.
- [17] S. Y. Zhang, W. Shi, P. Cheng, M. J. Zaworotko, *J. Am. Chem. Soc.* **2015**, *137*, 12203-12206.
- [18] X. T. Rao, T. Song, J. k. Gao, Y. J. Cui, Y. Yang, C. D. Wu, B. L. Chen, G. D. Qian, *J. Am. Chem. Soc.* **2013**, *135*, 15559-15564.
- [19] G. Y. Jin, Z. J. Liu, H. F. Sun, Z. Y. Tian, *Luminescence* **2016**, *31*, 190–194.
- [20] X. J. Li, S. Lu, D. Tu, W. Zheng, X. Y. Chen, *Nanoscale* **2020**, *12*, 15021-15035.
- [21] C. Yu, Fei. Chen, X. B. Yin, *Biosens. Bioelectron.* **2019**, *135*, 208-215.
- [22] X. Y. Xu, X. Lian, J. N. Hao, C. Zhang, B. Yan, *Adv. Mater.* **2017**, 1702298.
- [23] A. S. Rad. M. Ardjmand. M. R. Esfahani. B. *Spectrochim. Acta A.* **2021**, *247*, 119082.
- [24] Y. Zhao and D. Li. *J. Mater. Chem. C.* **2020**, *8*, 12739-12754
- [25] Y. Zhang, B. Li, H. Ma, L. Zhang, Y. Zheng, *Biosens. Bioelectron.* **2016**, *85*, 287-293.

For table of content only



Luminescence detection is a fast and convenient method to quantify and control the drug amount in body fluids. Here, we present a new mixed lanthanide-based MOF that can selectively distinguish and monitor the amount of favipiravir among other potential COVID-19 drugs.

